LA-UR- 09-01727

Approved for public release;
distribution is unlimited.

Title:	Generating Relevant Kinetic Monte Carlo Catalogs Using Temperature Accelerated Dynamics with Control over the Accuracy.
Author(s):	Abhijit Chatterjee, Z # 224865, T-1/T-Division Arthur Voter, Z # 094620, T-1/T-Division
Intended for:	Journal of Chemical Physics.

Form 836 (7/06)

GENERATING RELEVANT KINETIC MONTE CARLO CATALOGS USING TEMPERATURE ACCELERATED DYNAMICS WITH CONTROL OVER THE ACCURACY

Abhijit Chatterjee and Arthur F. Voter*

Theoretical Division, Los Alamos National Laboratory, Los Alamos, New Mexico 87545

Francesco Montalenti

Dipartimento di Scienza dei Materiali, Università di Milano Bicocca,

Via R. Cozzi 53, I-20125 Milano, Italy

Abstract

We develop a variation of the temperature accelerated dynamics (TAD) method, called the p-TAD method, that efficiently generates an *on-the-fly* kinetic Monte Carlo (KMC) process catalog with control over the accuracy of the catalog. It is assumed that transition state theory is valid. The p-TAD method guarantees that processes relevant at the timescales of interest to the simulation are present in the catalog with a chosen confidence. A confidence measure associated with the process catalog is derived. The dynamics is then studied using the process catalog with the KMC method. Effective accuracy of a p-TAD calculation is derived when a KMC catalog is reused for conditions different from those the catalog was originally generated for. Different KMC catalog generation strategies that exploit the features of the p-TAD method and ensure higher accuracy and/or computational efficiency are presented. The accuracy and the computational requirements of the p-TAD method are assessed. Comparisons to the original TAD method are made. As an example, we study dynamics in sub-monolayer Ag/Cu(110) at the time scale of seconds using the p-TAD method. It is demonstrated that the p-TAD method overcomes several challenges plaguing the conventional KMC method.

Keywords: Accelerated Molecular Dynamics, Temperature Accelerated Dynamics, confidence measures, on-the-fly kinetic Monte Carlo, multiscale modeling

*Corresponding author: afv@lanl.gov

I. INTRODUCTION

The kinetic Monte Carlo (KMC) method [1–4] is a powerful materials modeling tool for studying dynamics as well as equilibrium properties of thermally activated processes [5, 6]. Due to its lower computational requirements than other atomistic methods, such as molecular dynamics (MD), it is routinely possible to perform KMC simulations of 10^6 or more atoms. KMC method can also reach time scales that are significantly larger than those accessible to MD. Conventional KMC schemes require a catalog of *relevant* processes to be known *a priori* for the given material system. Here, the term "relevant process" implies a process that is selected in a KMC simulation with probability that is greater than the statistical error at the time scales of interest to the simulation. Typically, the processes in a KMC catalog are guessed assuming the underlying kinetic mechanisms. In addition, the lattice approximation is often made in KMC, i.e., atoms reside in fixed lattice positions. While the lattice approximation simplifies the bookkeeping of atomic positions, it is often a poor assumption in many technologically-relevant materials, such as multicomponent materials and materials with spatially varying strain. Furthermore, since it is difficult to guess most concerted processes, as a general practice, concerted processes are disregarded in a KMC catalog. However, it has been demonstrated that concerted moves can play an important role in the dynamics even in simple systems [7]. The typical KMC catalog is incomplete because of these assumptions, which can result in inaccurate dynamical evolution and possibly unrealistic behavior.

Since the 1980s efforts have been made to perform KMC calculations in a more systematic way with reasonable assumptions. In Ref. [8], atomic processes prevalent at short timescales were detected using the MD method for any arbitrary potential energy surface. However, more efficient KMC catalog generation methods are needed in solid-state materials, where activation barriers can be large and processes can occur over long timescales. In the adaptive KMC method [7], the dimer method [9] is used to perform multiple random searches for processes from a potential energy basin that can take the system to other basins. The adaptive KMC method can correctly find many of the processes including concerted process without employing the lattice approximation. In the self-learning KMC method [10], the process catalog is generated using the "drag" method to calculate rates for pre-determined mechanisms. The lattice approximation was employed in Ref. [10]. Clearly, the KMC

catalogs obtained using these approaches overcome some of the assumptions inherent in conventional KMC catalogs. However, these approaches do not guarantee that relevant processes have been found and do not quantify the error associated with the KMC catalog. As a result, there is little control over the accuracy of the system dynamics.

A relevant KMC catalog can be generated with control over its accuracy by studying the true dynamics of the system. This task is performed efficiently using accelerated MD methods (see Ref. [11] and the references therein), such as the temperature accelerated dynamics (TAD) method [12]. The TAD method has been successfully employed to perform long timescale accelerated MD simulations for rare-event dynamics. While the MD method [13] can access up to 1 μs, the TAD method can routinely access timescales beyond 1 ms [11]. The TAD method has been applied to the study of solid-state materials ranging from metals to oxides, for e.g., in studies on surface science and epitaxial growth [12, 14–17] to evolution of defects in irradiated materials [18, 19]. In addition, a parallel implementation of the TAD method has been developed recently enabling simultaneous access to large length and time scales [15]. The major strengths of the TAD method include accurate dynamics, a large computational speed-up for infrequent events, and control over the accuracy and computational boost by employing confidence measures.

Another important feature of the TAD method is that it provides a connection between the MD and KMC method while overcoming the timescale problem. In the TAD method, a basin-constrained MD (BCMD) calculation is performed for a particular potential energy basin at a temperature higher than the system temperature (see Ref. [12] for definition of potential energy basin). Since the dynamics of activated processes is faster at high temperatures, one can detect processes from a basin more efficiently than at the actual system temperature. Each time the system escapes from the basin, the MD trajectory is returned to the same basin to search for more processes until a confidence criterion is satisfied in the TAD simulation. A KMC catalog is thus automatically generated by detecting and recording transitions. Hereafter, we refer to the TAD method of Ref. [12] as the original TAD method.

So far, the TAD method has not been employed to generate a KMC catalog. In this paper, we develop a variation of the TAD method called the p-TAD method that is designed to generate an *on-the-fly* KMC catalog accurate to a user-specified p-TAD confidence. The "p" in p-TAD denotes process catalog. The system evolution is studied by sampling processes

from the KMC catalog using a KMC algorithm. The *on-the-fly* KMC catalog evolves as new processes are added to the process catalog each time a new potential energy basin is visited. In addition, when a basin is revisited, processes from the basin relevant at the time scales of the p-TAD calculation are also added to the KMC catalog.

The outline of the paper is as follows. In Section II, a short overview of the original TAD method is given. In Section III, the p-TAD algorithm is described. Confidence measures for p-TAD process catalogs are derived. Comparisons to the original TAD method are made. In Section IV, the additional improvements in the p-TAD method are discussed, which help overcome error resulting from the harmonic transition state assumption made in the TAD method and improve the p-TAD computational efficiency. Different strategies for generating KMC catalogs with varying accuracy and computational requirements are discussed. Issues that arise while reusing a KMC catalog and the associated accuracy are also discussed. In Section V, the KMC catalog accuracy and the computational boost using the p-TAD method are assessed by studying Ag/Ag(100). In Section VI, the p-TAD method is employed to study dynamics in a relatively more complex system, namely, sub-monolayer Ag/Cu(110). This study highlights the strengths of the p-TAD method in comparison to the typical KMC schemes. Finally, the conclusions are presented in Section VII.

II. THE ORIGINAL TAD METHOD AND THE STOP CRITERION

The original TAD method [12] is a statistically correct and efficient algorithm for studying rare-event dynamics. A BCMD calculation is performed for a particular potential energy basin B at a temperature T_H in the canonical (NVT) ensemble. Here $T_H > T_L$ and T_L is the original system temperature. In this paper, subscripts H and L denote the high and low temperatures, respectively. A transition to a neighboring basin is detected every once a while in the BCMD calculation. Typically, the dynamics of activated processes is faster at higher temperatures. Consequently, the escape time for a process is significantly smaller at temperature T_H than at temperature T_L. It is assumed that the escape time τ_i for a process i with rate k_i at a given temperature T, i.e., the time τ_i spent in a particular basin before process i is observed, satisfies the exponential distribution [20]

$$f(\tau_i) = k_i exp(-k_i \tau_i). \tag{1}$$

It is also assumed that harmonic transition state theory (HTST) applies, so that the process rate is given by Arrhenius dynamics [6, 21]

$$k_i = \nu_i exp(-\beta E_i). \tag{2}$$

Here ν_i and E_i are the rate prefactor and activation barrier for process i, respectively, and $\beta = (k_B T)^{-1}$.

A high temperature escape time $\tau_{i,H}$ recorded in the BCMD simulation for process i in basin B is extrapolated to obtain the low temperature escape time $\tau_{i,L}$ such that

$$\tau_{i,L} = \tau_{i,H} exp(-E_{a,i}(\beta_L - \beta_H)). \tag{3}$$

Eq. (3) can be derived from Eqs. (1) and (2). This extrapolation is necessary for obtaining the correct system dynamics at temperature T_L. Eq.(3) is plotted in Fig. 1a as dashed lines with slope equal to $-E_i$ (see Ref. [12] for more details). Each time a transition from the basin B is observed, the extrapolated low MD escape time is recorded and the trajectory is returned to the same basin B. Fig. 1 shows an Arrhenius-like diagram for the TAD calculation in basin B where the inverse escape times (semilog y-axis) are plotted against the inverse temperature (more correctly β) along x-axis. As shown in Fig. 1a, a sequence of projected low temperature escape times are recorded for the basin. Multiple extrapolated times can be recorded for the same process in the basin B. The TAD method specifies a high temperature stop time $t_{H,stop}$ (defined below) for the BCMD calculation during which escape times are recorded. The stop time depends on the shortest low temperature escape time. Once the time $t_{H,stop}$ is reached in the BCMD calculation, it is guaranteed with a confidence level $1 - \delta_{TAD}$ that no future BCMD transitions will have a extrapolated low temperature escape time that is shorter than the current shortest escape time. The event with the shortest time is identified, the corresponding process is selected and the system jumps to a different basin B' determined by the selected process. The clock is advanced by the shortest low temperature escape time in B. A new BCMD calculation is performed in the basin B' and the aforementioned procedure is repeated.

Consider a BCMD simulation where the current shortest low temperature escape time from all processes in B is $t_{L,short}$. The stopping time for the original TAD method is given by [12]

$$t_{H,stop} = \frac{(\nu^*_{TAD} t_{L,short})^{\beta_H/\beta_L}}{\nu^*_{TAD}}. \tag{4}$$

Here $\nu^*_{TAD} = \nu_{min}/ln(1/\delta_{TAD})$ and ν_{min} is an assumed lower bound for the rate prefactor for all possible transitions. Typical values of ν_{min} range from $10^{11} - 10^{12}$ s^{-1}. Eq.(4) corresponds to the solid line with the y-intercept being ν^*_{TAD} in Fig. 1a. The term ν^*_{TAD}, which is fixed in the original TAD calculation once values of ν_{min} and δ_{TAD} are specified, is called the original TAD pivot since the stop line pivots about this point. The intersection of this line with the vertical line at β_H gives the time $t_{H,stop}$. Note that the BCMD duration of $t_{H,stop}$ is significantly smaller compared to the MD duration $t_{L,short}$ since the exponent $\beta_H/\beta_L < 1$ in Eq.(4). This explains the higher computational efficiency of the original TAD method compared to MD.

Other variations of the TAD method have also been developed. When a basin B is revisited, the BCMD simulation can proceed from where it stopped in the previous visit by using the unused sequence of recorded low temperature escape times [14]. This increases the efficiency of the TAD method for revisited states since the escape times for many processes are now already known without repeating the expensive BCMD calculation at the current time scales. More importantly, based on the computed value of $t_{H,stop}$ it is observed that unlike the original TAD method the average duration for the BCMD calculation for each basin revisit gets progressively shorter with more basin revisits. This effect, referred to as the "pivot" effect, is also observed in the p-TAD method as described in more detail in the next section. A more efficient TAD stop criterion compared to Eq. (4) was developed in Ref. [14] where it was assumed that a lower bound for all process activation barriers for a particular potential basin, denoted by E_{min}, is known along with ν_{min}. Another variation of the TAD method called the synthetic TAD method was developed for studying material systems with a separation of time scales resulting from fast and slow processes [12]. In the synthetic TAD method, when certain processes from a basin B are selected more frequently compared to others in a TAD calculation, the former are denoted as synthetic/fast processes. A sequence of low temperature escape times is sampled from Eq.(1) (without performing any BCMD calculations) for the synthetic processes. The rates for the synthetic processes at temperature T_L are needed for generating the sequence of synthetic escape times. Thereafter, only escape times of slow processes are projected in the high temperature BCMD calculation. After several revisits to a basin, it can be observed that often times the shortest escape time can be detected with a very short BCMD calculation based on the stop criterion due to the pivot effect. As shown next, the p-TAD method samples escape time for all processes, slow

and fast, from Eq.(1), and has the same advantages as the synthetic TAD method. However, the p-TAD method has differences from previous TAD methods, which results in a higher accuracy.

III. THE P-TAD METHOD

A. Algorithm

The p-TAD method, like the original TAD method, is a statistically correct and efficient algorithm for studying rare-event dynamics. A high temperature BCMD calculation is performed to efficiently detect processes from the current basin B. It is assumed that Eq. (1) is obeyed. In the p-TAD method, unlike the original TAD method, the high temperature escape time is not extrapolated to obtain the low temperature dynamics. Instead, a KMC algorithm is used to study the dynamics. When a new process i is detected in the basin, it is added to the existing list of relevant processes for the basin B. The escape time $\tau_{i,L}$ for process i at temperature T_L is randomly sampled from Eq. (1). This is shown schematically in Fig. 1b. The low temperature process rate is needed for sampling the time $\tau_{i,L}$. Note that Eq. (2) is not required. Discussion on different approaches for estimating the low temperature process rates and the resulting improvement in the accuracy of the p-TAD method compared to the original TAD method is given in Section IV.

Instead of directly using the time $\tau_{i,L}$, the cumulative time $t_{i,L}$, which is the sum of escape times $\tau_{i,L}$ for the process i in basin B, is used. When the process i is detected for the first time, the low temperature escape time is

$$t_{i,L} \leftarrow \tau_{i,L}. \tag{5}$$

In the first visit to B, the escape time of all processes in B is given by Eq. (5). Note that analogous to the KMC method, each process has only one escape time (see example in Fig. 1b). This is in contrast to the original TAD method where multiple escape times can be recorded for a single process. The process I with the shortest escape time $t_{I,L}$ out of all processes from the basin B is identified. This is shown schematically in Figs. 1a and 2. The p-TAD algorithm specifies a stop criterion for the BCMD calculation, given by the BCMD stop time $t_{H,stop}$ (derived below), that guarantees with a user-specified confidence $1-\delta$ that all processes from basin B that are relevant at the time scales $t_{I,L}$ have been found. The

time $t_{H,stop}$ depends on the shortest escape time $t_{I,L}$. The BCMD calculation is performed till the BCMD time reaches $t_{H,stop}$. It is possible that a new process I' is detected with an escape time $t_{I',L} < t_{I,L}$ before the stop time is reached. In such as case, the time $t_{H,stop}$ is recomputed from time $t_{I',L}$. Once the stop criterion is satisfied, the process J with the shortest escape time $t_{J,L}$ is selected and the system escapes to the corresponding basin B'. The clock is advanced by time $\tau_{J,L}$. A new cumulative escape time

$$t_{J,L} \leftarrow t_{J,L} + \tau_{J,L} \tag{6}$$

is sampled for selected process J in basin B, which is used for a future visit to basin B. Here $t_{J,L}$ on the right hand side of Eq. (6) is the previous cumulative time and $\tau_{J,L}$ is the newly sampled low temperature escape time for process J. When the basin B is revisited, the low temperature escape times for processes that were not selected in the previous visit and the new escape time for process J from Eq. (6) are used (see illustration in Fig. 2). A new time $t_{H,stop}$ is computed based on these escape times. As more time is spent in basin B additional processes are added to the KMC catalog.

B. Confidence measures

The confidence measure for the original TAD method guarantees with the chosen confidence level that the shortest low temperature escape time has been found. On the other hand, the p-TAD method guarantees with the chosen confidence that processes that are relevant at the current time scale of the simulation have been detected. Consequently, the derivation and mathematical form of the p-TAD stop criterion differs from the original TAD stop criterion.

Consider a BCMD simulation where the shortest low temperature escape time from all processes in the basin B is $t_{L,short}$. The time $t_{L,short}$ can be set arbitrarily high when a basin is visited for a first time and no process has been detected yet. Integrating Eq. (1) in time for a process with rate k, the probability that the escape time for this process is shorter than $t_{L,short}$ is given by

$$p_{ma} = 1 - exp(-kt_{L,short}). \tag{7}$$

A value of p_{ma} close to 1(0) implies that the process will be frequently (rarely) observed at low temperature time scales $t_{L,short}$. The subscript "ma" denotes that the process matters,

i.e., it is relevant to the KMC catalog. Similarly, the probability that the escape time for the same process is longer than time $\alpha t_{L,short}$ is

$$p_{mi} = exp(-\alpha k t_{L,short}). \tag{8}$$

The subscript "*mi*" denotes the process would be missing from the catalog. Fig. 3a shows the behavior of p_{ma} and p_{mi} for any process in terms of dimensionless time kt. The probability p_{ma} is nearly 0 at short times ($O(kt_{L,short}) \ll 1$). Here $O()$ denotes order of magnitude. The probability p_{ma} increases with time. At longer times when $O(kt_{L,short}) \sim 1$, p_{ma} approaches 1, indicating that the process is relevant at those times. The probability p_{mi} depends on the value of α. At short times ($O(\alpha k t_{L,short}) \ll 1$), p_{mi} is nearly 1 indicating that the process might be missing in the KMC catalog. Eventually, p_{mi} approaches a value of 0 at longer times. The probability of a process that is relevant at time $t_{L,short}$ and is missing from the catalog till low temperature time $\alpha t_{L,short}$ yields an error measure

$$\epsilon = p_{ma} p_{mi} = (1 - exp(-kt_{L,short}))exp(-\alpha k t_{L,short}) \tag{9}$$

for the process. In Fig. 3a, the error measure is plotted against time for $\alpha = 5$ and 40. A maximum in ϵ is observed. Processes with $kt_{L,short} \ll 1$ (to the left of the maximum) will have a low value of p_{mi} and are most likely already present in the process catalog. On the other hand, processes with $kt_{L,short} >> 1$ (to the right of the maximum) will have a low value of p_{ma} and are not required to be present in the process catalog. Such types of processes have small error contributions to the KMC catalog. The maximum in the error measure implies that for a given time $t_{L,short}$ a corresponding worst case process rate k_w (subject to the value of α used) can be identified such that a process with the rate k_w will be the biggest contributor to the error. Here the subscript w denotes the worst case. The rate k_w is obtained by solving $d\epsilon/dk = 0$, which gives

$$k_w = \frac{1}{t_{L,short}} ln \frac{\alpha_w + 1}{\alpha_w}. \tag{10}$$

Given the value of α, the corresponding error is obtained by inserting the value of k_w in Eq. (9) as shown in Fig. 3a. Alternatively, it is more useful to estimate α_w where the maximum error equals δ, such that $0 < \delta < 1$. We refer to $1 - \delta$ as the confidence measure, which is used in the p-TAD method as a parameter to control the accuracy of the KMC catalog. As an example, $\delta = 0.01$ implies 99% confidence. From Eqs. (9) and(10)

$$\delta = \frac{\alpha_w^{\alpha_w}}{(\alpha_w + 1)^{\alpha_w + 1}}, \tag{11}$$

which is solved numerically to obtain the value of α_w in terms of δ. We term α_w as the horizon, since only processes detected up to time $\alpha_w t_{L,short}$ are deemed relevant to the KMC catalog for the chosen confidence $1-\delta$. Fig. 3b shows that the horizon α_w increases as the confidence levels increase. The contributions from both $p_{mi,w}$ and $p_{ma,w}$ decrease with increasing confidence. Note that $p_{ma,w}p_{mi,w} = \delta$.

When $\delta \ll 1$, the value of α_w is large and Eq. (10) is approximated as

$$k_w \approx \frac{1}{t_{L,short}} \ln \frac{\alpha+1}{\alpha} \approx \frac{1}{\alpha_w t_{L,short}}. \tag{12}$$

From Eq.(11),

$$\alpha_w = (\delta e)^{-1}, \tag{13}$$

where e is base of the natural logarithm. An infinitely long horizon is required as the confidence level approaches 1. When $\delta = 0.01$, one gets $\alpha_w \approx 36.3$, $k_w t_{L,short} \approx \alpha_w^{-1} = 0.027$, $p_{mi,w} \approx e^{-1} = 0.37$ and $p_{ma,w} \approx \alpha_w^{-1} = 0.027$. Since the average escape time for an exponential process with rate k is $\langle t_{escape} \rangle = 1/k$, the value of $k_w t_{L,short} = 0.027$ indicates that the worst case rate k_w corresponds to a process with average escape time much larger than $t_{L,short}$.

C. Stop criterion

Next a stop criterion is derived by projecting the low temperature time $\alpha_w t_{L,short}$ to obtain a high temperature stop time $t_{H,stop}$. Note that the high temperature stop criterion can be directly checked in the BCMD calculation by following the BCMD time. Since Eq. (1) is valid for both T_L and T_H, a correct distribution for τ_H is obtained from a given distribution of escape time τ_L when

$$\tau_H = k_{w,L}\tau_L / k_{w,H}. \tag{14}$$

Since there can always be a (real/hypothetical) process with worst case rate k_w that has not been detected yet in the BCMD simulation, one gets $\tau_H = t_{H,stop}$ and $\tau_L = \alpha_w t_{L,short}$ for such a process. From Eq. (14), the BCMD stop time in terms of the unknown activation barrier E_w satisfies

$$t_{H,stop} = \alpha_w t_{L,short} exp(-(\beta_L - \beta_H)E_w). \tag{15}$$

when Arrhenius dynamics (Eq. (2)) is assumed. The time $t_{H,stop}$ is large when E_w is small. In turn, E_w is small when ν_w is small, since $k_w = \nu_w exp(-\beta_L E_w)$. As in the original TAD

method, we assume that the lower bound for process rate prefactor is ν_{min}. This gives an upper bound for time $t_{H,stop}$. The lower bound for the activation barrier is

$$E_{w,min} = \frac{1}{\beta_L} ln \frac{\nu_{min}}{k_w} \tag{16}$$

and BCMD stop time is

$$t_{H,stop} = \frac{(\nu^*_{p-TAD} \alpha_w t_{L,short})^{\beta_H/\beta_L}}{\nu^*_{p-TAD}}. \tag{17}$$

Here $\nu^*_{p-TAD} = \nu_{min}/ln(1/p_{mi})$. For a given T_L, $t_{L,short}$, ν_{min} and δ, Eq.(17) corresponds to a straight line given by

$$ln(1/t_{H,stop}) = ln(\nu^*_{p-TAD}) - \frac{\beta_H}{\beta_L} ln(\nu^*_{p-TAD} \alpha_w t_{L,short}). \tag{18}$$

in Fig. 1b with a y-intercept of ν^*_{p-TAD}. The stop criterion pivots about the p-TAD pivot ν^*_{p-TAD}. This behavior is called the pivot effect. The p-TAD pivot is fixed once ν_{min} and δ are known. The intersection of the stop line with the vertical line through β_H gives the stop time. A shorter stop time results in lower CPU requirements. For a given $t_{L,short}$, the stop time is small when the pivot ν^*_{p-TAD} is large and the horizon α_w is small (large ν_{min} and small δ). The stop time is also small for a small value of the exponent β_H/β_L.

From Eq. (17), the duration of BCMD calculation needed for low temperature dynamics from time $t_{L,1}$ to $t_{L,2}$ is proportional to $t_{L,2}^{\beta_H/\beta_L} - t_{L,1}^{\beta_H/\beta_L}$(see Fig. 2). As evident from Eq. (17), the duration of BCMD calculation for basin revisits decreases in a power-law fashion as more time is spent in the basin B due to the pivot effect. This can also be concluded from the derivative $dt_{H,stop}/dt_{L,short}$ which is proportional to $1/t_L^{1-\beta_H/\beta_L}$, where $\beta_H/\beta_L < 1$. This feature of a p-TAD, which is also common to other TAD methods [14], exploits basin revisits to gain computational efficiency. As a consequence, the p-TAD computational requirements per unit time of the low temperature dynamics becomes smaller as more time is spent in a given basin.

For all values of δ, $\nu^*_{p-TAD} > \nu^*_{TAD}$ when $\delta = \delta_{TAD}$. This is shown schematically in Fig. 1a and b through the position of the respective pivots. For small values of δ, the value of p_{mi} converges to a value of e^{-1} and $\nu^*_{p-TAD} \approx \nu_{min}$. For larger values of δ, $\nu^*_{p-TAD} > \nu_{min}$. This is in contrast to the original TAD method where the value of ν^*_{TAD} becomes smaller than ν_{min} below a certain δ_{TAD}. More discussion on the computational boost from the p-TAD method compared to the MD method is given in Sec. V.

D. Sweeping effect and the swept time

Instead of estimating the stop time, one can estimate the low temperature time for which the KMC catalog is accurate to the chosen confidence $1-\delta$ when the duration of BCMD calculation in basin B is known. In this case, the low temperature time increases in a power-law fashion with respect to BCMD time. This behavior is termed the sweeping effect. The estimated low temperature time $t_{L,swept}$ that is "swept" from the total BCMD time t_H spent in the basin B is obtained by rearranging Eq. (17) and is given by

$$t_{L,swept} = \frac{(\nu^*_{p-TAD} t_H)^{\beta_L/\beta_H}}{\alpha_w \nu^*_{p-TAD}}. \tag{19}$$

This is shown in the example in Fig. 3a where the swept time increases by three orders of magnitude for each order of magnitude BCMD time. The swept time plotted in the figure are 10^{-6}, 10^{-3} and 10^{0} s. The value $\alpha t_{L,swept}$ is plotted, where $\alpha = 1/\delta e$. As evident from Eq. (19), the sweeping effect becomes more aggressive for large values of the exponent β_L/β_H and the pivot ν^*_{p-TAD}.

The p-TAD method naturally allows the use of parallel processors to generate a KMC catalog. Consider the case where m processors are employed to perform m BCMD calculations for the same basin B using different random number seeds. Each processor generates a KMC catalog till time t_H with a confidence level $1-\delta$. The m KMC catalogs are merged. The total high temperature BCMD time accessed is mt_H. From Eq. (19), the merged process catalog is accurate to a confidence level $1-\delta$ for an effective swept low temperature time that is proportional to $(mt_H)^{\beta_L/\beta_H}$ and not just $mt_H^{\beta_L/\beta_H}$. The computational speed-up resulting from the combination of sweeping effect with parallel computing becomes evident through an example where $\beta_L/\beta_H = 3$ and $m = 100$. In this case, the contribution from the term m^{β_L/β_H} is 10^6!

IV. IMPROVING P-TAD ACCURACY & REUSING PROCESS CATALOGS

A. Rate estimation methods

Anharmonicity errors are encountered in the original TAD method when the harmonic approximation in Eq. (2) breaks down. As a result, the extrapolated time at temperature T_L using Eq. (3) can be incorrect. The anharmonicity error in original TAD method is

largest when temperature T_H is large and significantly different from temperature T_L [12]. In contrast, the high temperature BCMD calculation is used in the p-TAD method to detect only the relevant processes for the basin. The correct process rate at T_L can be computed accurately (without the anharmonicity error) and it can be used to sample the correct distribution of escape times from Eq. (1). As in the original TAD method, the p-TAD method still assumes that long-ranged anharmonic effects at temperature T_H, such as, volume expansion effects and phase transformations, do not alter the underlying process mechanisms [12].

A combination of different approaches available in the literature, entailing rate estimation technique as well as the details of the potential energy surface (PES), can be employed to obtain accurate process rates. This is not possible with the previous variations of the TAD method outlined in Section II and in typical MD calculations. For example, the transition state theory (TST) rate can be computed with dynamical corrections whenever extremely accurate dynamics is desired. Although TST rate estimation can be computationally expensive, which can limit the length and time scales accessible to the simulation, the rate is estimated only when a new process is detected. Alternatively, approximate process rates can be efficiently estimated from the Vineyard equation (harmonic TST, Eq. (2)). The activation barriers are estimated using the Nudged Elastic band (NEB) method [22]. The HTST rates are used for the p-TAD calculations in Section V and VI.

The uncertainty in the process rates can be significant when an empirical potential, such as embedded atom method, is employed. Once a new process has been detected with the BCMD calculation using an empirical potential, accurate low temperature rates can be estimated from a higher quality potential energy surface. Examples include density functional theory (DFT) method [23, 24] with the HTST approximation or ab initio MD simulations [25]. Here is it assumed that the low and high quality potential energy surface (PES) conform to each other, i.e., the same process mechanisms are observed on both PES. As a result, even quantum effects, such as tunneling, can be captured accurately with the p-TAD method. A similar strategy can also be employed when an empirical interaction potential is fitted for only certain types of local atomic environments. The interaction potential typically becomes unreliable when a local environment is encountered that is not included in the fit. In such a case, one can employ the empirical potential for environments included in the fit and perform higher quality PES calculations elsewhere.

B. Anharmonicity allowance & Automatic corrections

Whenever the escape time of a process i that is currently missing from the KMC catalog is shorter than the current time $t_{L,short}$, a process other than the missing process i is selected by the p-TAD method. This can lead to an error in the p-TAD dynamics. The error can be categorized as sampling and anharmonicity error. A sampling error occurs when a missing process that is not relevant to the KMC catalog for the chosen confidence level has the shortest sampled escape time. This behavior is witnessed rarely when the rate for the missing process is small, i.e., $O(kt_{L,short}) \ll 1$, where k is the low temperature rate of the missing process. Sampling errors can be made statistically insignificant in comparison to the uncertainty in the interaction potential parameters by choosing sufficiently high confidence levels (see example in Section V). The effect of the unceratinity in time $t_{L,short}$ on the p-TAD based KMC catalog accuracy can also be reduced by using high confidence levels. The anharmonicity error in p-TAD method has a source different from the one in the original TAD method discussed previously. Under certain circumstances (see Fig. 4b) relevant processes that display anharmonic effects can be missing from the KMC catalog due to an incorrect stop time. In cases when $O(kt_{L,short}) \approx 1$ and the resulting error in the dynamics can be significant. The anharmonicity error can be prevented by introducing an anharmonicity allowance f that allows for error made while estimating time $t_{H,stop}$. The resulting expression for the high temperature stop time

$$t_{H,stop} = \frac{(\nu^*_{p-TAD}\alpha_w f t_{L,short})^{\beta_H/\beta_L}}{\nu^*_{p-TAD}}, \tag{20}$$

generates the correct KMC catalog for the chosen confidence level once the value of f is known for a basin. It should be noted that the value of f depends on missing processes relevant at the time scale of the simulation. Since the missing processes are not known *a priori*, a value of anharmonicity allowance can be estimated from the largest value of f computed based on observed processes in the visited basin(s). In such a case, the anharmonicity allowance is given by

$$f = \max_{all\ processes}(k/k_{Vineyard}, k_{Vineyard}/k), \tag{21}$$

where k is the actual process rate at high temperature and $k_{Vineyard}$ is the process rate from Vineyard expression. Equations derived earlier can be used directly by substituting $t_{H,stop}$ with $t_{H,stop}/f$. Hereafter, it is assumed that $f = 1$.

While the anharmonicity allowance improves the accuracy of the p-TAD method it is difficult to predict f for a particular basin and time scale. Relevant processes could still be missing from the process catalog when f is underestimated. On the other hand, the p-TAD calculation becomes more expensive when f is overestimated since time $t_{H,stop}$ is longer. The p-TAD method can in fact correct the dynamics by itself when a missing relevant process is detected for any value of f. Consider the case where a new process I is observed during a basin revisit and the escape time $t_{I,L}$ sampled for process I from Eq. (6) is shorter than the current time spent in the basin. In this case, the process I has the shortest escape time and is selected. The dynamics can then proceed from the time $t_{I,L}$ in the past with a more accurate process catalog. As a result, the error from an underestimated value of the anharmonicity allowance is automatically corrected. Such instances, where time switches back to the past, were witnessed thrice in Ag/Cu(110) p-TAD calculations of Section V when confidence levels were low ($\delta = 0.1$). It is possible that a KMC trajectory spends significant time in other basins while processes from those basins are added to the KMC catalog. Eventually, the trajectory can return to the past upon detecting a missing process during a basin revisit. As a result, this approach can be computationally inefficient since a higher accuracy KMC catalog is generated than desired. To avoid such a case, one may use a higher confidence level whenever frequent jumps to the past are observed. Alternatively, approximations can be introduced into the catalog generation procedure. For instance, when δ is small and a jump to the past is attempted, the system time is simply not modified. This assumption has been made for most p-TAD calculations in this paper.

C. Reusing KMC catalogs & effective confidence

In the original TAD method, multiple BCMD calculations are required to generate different sequences of escape times for collecting non-equilibrium statistics. This can be implemented using different random number generator seeds with the thermostat or by randomly perturbing the initial conditions. In contrast, a p-TAD based KMC catalog can be used directly with the KMC method for generating the statistics without performing any additional expensive BCMD calculations. Here it is assumed that the basins visited in the KMC simulations are same were also visited in the p-TAD calculation that generated the process catalog. Reusability of p-TAD based KMC catalogs improves the p-TAD efficiency while

generating ensemble statistics with a control over the accuracy.

A p-TAD based KMC catalog can be employed for conditions different from the one it was generated for assuming that the same process mechanisms are present at the new conditions. The process rates are recomputed for the new conditions. Approximate effective confidence levels/error for process catalog are derived directly from Eq.(19) by solving

$$\frac{\alpha\nu^*_{p-TAD}t_{L,swept}}{(\nu^*_{p-TAD}t_{H,stop})^{\beta_L/\beta_H}} = \frac{\alpha\nu^*_{p-TAD}t_{L,swept}}{(\nu^*_{p-TAD}t_{H,stop})^{\beta_L/\beta_H}} \tag{22}$$

numerically. Here the prime denotes values at the new conditions. The parameter values δ, ν_{min}, $t_{L,swept}$ and T_L can be different for the two conditions. Analytical expressions are derived when $\delta, \delta' \ll 1$, $\nu_{min} = \nu_{min'}$ and $1/\alpha = \delta e$. When a KMC catalog, which is accurate to confidence $1-\delta$ till time $t_{L,swept}$, is frozen, i.e., it is not updated any longer, the effective error is

$$\delta' = \delta(t'_{L,swept}/t_{L_swept}) \tag{23}$$

if the catalog is used till a different time $t'_{L,swept}$ at the same temperature. As expected the error δ' is less (greater) than the original error when time $t'_{L,swept}$ is less (greater) than $t_{L,swept}$. Furthermore, the error δ' increases linearly with time $t'_{L,swept}$ as long as $\delta' \ll 1$. When a KMC catalog valid till time $t_{L,swept}$ at temperature T_L is used at a different temperature T'_L for the same time $t_{L,swept}$, the effective error is

$$\delta' = \delta(\nu_{min}t_{H,stop})^{(\beta_L-\beta'_L)/\beta_H} \tag{24}$$

In this case, the error is small when $T'_L < T_L$.

A previously generated p-TAD based KMC catalog can be refined further with p-TAD method. Effective confidence levels derived above give the resulting confidence associated with the new catalog. Other KMC catalog generation methods, such as the adaptive KMC method, can complement the p-TAD method in detecting missing processes, while the p-TAD method specifies the confidence level for the KMC catalog. The rates for previously detected processes can be used directly with the p-TAD method. This reduces the computational overhead associated with process rate estimation.

V. ACCURACY AND COMPUTATIONAL REQUIREMENTS

The diffusion of a Ag adatom on a Ag (100) surface is studied as a prototype system to assess the accuracy and computational requirements of the p-TAD method in terms of

the p-TAD confidence measure $1-\delta$ and the minimum prefactor ν_{min}. The system studied (shown in Fig. 5a)consists of 1 Ag adatom on 4 Ag moving (top) and 4 Ag fixed (bottom) layers. A total of 257 Ag atoms are present. Slab boundary conditions are employed.

The embedded-atom (EAM) potential of Ref. [26] is employed. The EAM potential parameters were fitted to both experimental and first-principles data for various Ag structures in Ref. [26]. In the same work, the potential was combined with an existing potential for Cu to obtain a Ag-Cu alloy EAM potential which demonstrated good agreement with experimental data.

It is known that a Ag adatom migrates on the Ag(100) surface typically via either a hop or an exchange mechanism [12], although other processes can also be encountered [14]. By performing translation operations and renumbering the atom indices, the system keeps revisiting the same potential energy basin after each Ag adatom hop/exchange move. A total of 1000 KMC events were studied with the p-TAD method during which 18 different types of processes, including symmetrically equivalent processes, were observed in the BCMD simulation. The activation barriers found for the hop and exchange mechanism are 0.51 and 0.72 eV, respectively. The prefactors obtained from the Vineyard equation are 5.4×10^{12} and $10^{11} s^{-1}$, respectively. It was observed in [12] using a Ag EAM potential different from the one employed here that the anharmonicity factor, i.e., ratio of the TST to HTST rate, can be 4 or more at $T = 700$ K for Ag/Ag(100). Despite this, for simplicity the anharmonicity factor f was taken to be 1. The total time t_L elapsed by the end of the 14 hour p-TAD calculation on a single processor was 0.12 ms with p-TAD parameters $T_H = 750$ K, $T_L = 400$ K, a friction factor of $10^{12}\ s^{-1}$, time step of 4 fs, confidence level of 99% ($\delta = 0.01$) and $\nu_{min} = 10^{12}\ s^{-1}$.

In Fig. 5b, the addition of the 4 symmetrically equivalent hop processes to the KMC catalog is studied for different conditions. In a single p-TAD calculation, the number of detected hop processes N after the n^{th} visit to the potential energy basin is an integer value. Initially, $N = 0$ when $n = 0$, since all processes in the basin are unknown. As more time is spent in the basin, the value of N increases to a maximum value of 4. Multiple p-TAD calculations were performed to obtain an average value $\langle N \rangle$ as a function of n by generating a separate KMC catalog from each p-TAD calculation. Here $\langle N \rangle$ denotes ensemble average. The average $\langle N \rangle$ is plotted in Fig. 5b. Averaging eliminates the discontinuity and noise present in a single p-TAD trajectory. Different random number seeds are used with the

BCMD Langevin thermostat. A total of 100, 60 and 40 p-TAD trajectories are used for $\delta = 0.2$, 0.1 and 0.01, respectively. Other p-TAD parameter values are mentioned in the figure caption. It is observed that all the hop processes are detected within the second basin visit when $\delta = 0.01$. On the other hand, even after 10 visits all hop processes are detected in only few of the 100 p-TAD trajectories. As mentioned earlier, it is not necessary for all processes to be the present in the KMC catalog when the dynamics is studied with the p-TAD method. However, in this case all the hop processes are equally relevant. Note that all hop directions are detected with the same probability for any value of δ in the p-TAD method, i.e. p-TAD is unbiased. The absence of some of the hop processes in the KMC catalog will lead to inaccurate dynamics. The absence of some of the hop processes when confidence level is low can be explained in terms of the value of α_w. The value of horizon α_w is 1.3, 3.1 and 34 for $\delta = 0.2$, 0.1 and 0.01, respectively. When $\delta = 0.2$ the horizon is too short for most of the relevant processes to be detected, i.e., sampling error is present. It is recommended to use $\delta < 0.05$ to ensure that the KMC catalog is accurate. Furthermore, strategies presented in SectionIV can be employed to correct the value of δ *on-the-fly* to improve the p-TAD accuracy. The average CPU time for $n = 10$ KMC moves was 12, 21 and 65 min for $\delta = 0.2$, 0.1 and 0.01, respectively.

The parameter ν_{min} can also control the p-TAD accuracy. In Fig. 5b, $\langle N \rangle$ is plotted for $\nu_{min} = 7.6 \times 10^{11}\ s^{-1}$ and $\delta = 0.2$ using 100 p-TAD calculations. The 4 hop processes are detected in fewer basin visits compared to when $\nu_{min} = 10^{12}$. This is because when the ν_{min} is small, the sweeping effect is less aggressive and BCMD stop times are large (see Eq. (17)). The same value of ν^*_{p-TAD} is obtained for $\nu_{min} = 7.6 \times 10^{11}\ s^{-1}$, $\delta = 0.2$ and $\nu_{min} = 10^{12}\ s^{-1}$, $\delta = 0.01$. Yet the detection of all the hop processes takes more visits in the former case. This is because the horizon α_w is shorter when $\nu_{min} = 7.6 \times 10^{11}\ s^{-1}$ and $\delta = 0.2$ resulting in a shorter stop time. This is contrary to observations made in the original TAD method where the stop time of two TAD runs are same for the same value of time $t_{L,short}$ and pivot ν^*_{TAD}. Though the original TAD method is not designed to generate KMC catalogs, one can still estimate $\langle N \rangle$ from an original TAD calculation. Fig. 5b shows that the confidence measures of original and the p-TAD method cannot be compared directly, i.e., when $\delta = \delta_{TAD}$ the number of processes in respective KMC catalogs can be vastly different. 100 original TAD calculations were used. The average original TAD CPU time when $\nu_{min} = 10^{12}\ s^{-1}$ and $\delta_{TAD} = 0.2$ is 33 min for $n = 10$ KMC moves.

The exact CPU requirements for a p-TAD calculation can be estimated from

$$CPU_{total} = t_{H,stop} \times CPU_{MD} + CPU_{overhead} + CPU_{KMC}. \tag{24}$$

Here CPU_{MD} is the computational requirements per unit time of MD performed. As the temperature T_H increases, the MD cost of the BCMD calculation in the p-TAD method (for time $t_{H,stop}$) decreases drastically compared to a typical MD calculation performed at system temperature T_L (for low temperature time t_L) due to the pivot effect. The computational overhead $CPU_{overhead}$ includes additional costs for detecting processes from the BCMD calculation, process rate estimation and KMC catalog update. The computational overhead depends on the relevant processes from the basin, the current time scale of the simulation and the p-TAD parameters. For e.g., the KMC process catalog update, which typically has low CPU requirements, can become expensive when several KMC processes have already been detected in the current basin and future BCMD transitions need to be classified as either new or observed processes by regularly comparing to the existing KMC catalog. The computational requirements associated with the KMC selection and update is given by CPU_{KMC}. The computational cost of the p-TAD method approaches that of a KMC method, i.e., the CPU cost is CPU_{KMC}, when the KMC catalog is already known for the time scales of interest and no further BCMD calculations are required.

It is evident from Eq. (24) that the p-TAD method is extremely efficient compared to the MD method when the boost

$$B_{p-TAD} = \frac{t_L}{t_{H,stop}} = \frac{(\nu^{\star}_{p-TAD} t_L)^{1-T_L/T_H}}{\alpha_w^{T_L/T_H}} \tag{25}$$

is large. Here it is assumed that the CPU requirements from overhead and KMC terms in Eq. (24), which are absent in MD, are small compared to the BCMD computational requirements. Eq. (25) shows that the boost obtained from the p-TAD method increases with time t_L. The boost increases for large ratio T_H/T_L, small δ and large ν_{min}. The boost obtained from the p-TAD method can often reach a value of 10^3 or more. This enables the p-TAD method to access timescales of milliseconds and higher, which is not possible with the MD method. In comparison, the boost in original TAD method is given by

$$B_{TAD} = (\nu^{\star}_{TAD} t_L)^{1-T_L/T_H}. \tag{26}$$

The crossover where the p-TAD method provides more boost in comparison to the original

TAD method occurs at $T_L/T_H \geq ln(a)/(a + ln(a) - 1)$ such that $\delta_{TAD} = \delta, \delta \ll 1$. Here $a = ln(1/\delta)$.

The CPU requirements for a 1000 KMC move p-TAD calculation of the Ag/Ag(100) system is shown in Fig. 6 for three different temperatures T_L = 200, 300 and 400 K. The BCMD calculation is performed at 750 K for the three temperatures using $\nu_{min} = 10^{12}\ s^{-1}$ and $\delta = 0.01$. Majority of the computational effort is required in performing the BCMD calculations. Consequently, the CPU time is proportional to the BCMD time. Note that the KMC catalog generated from one value of T_L can be directly used at the other low temperatures. In such a case the p-TAD computational costs reduce significantly. In Fig.6, it is observed that longer time scales are accessed for fixed computational requirements when temperature T_L is low. This is also evident from the exponent in Eq. (25). The p-TAD boost ranges from $10^3 - 10^{10}$ between temperatures T_L = 400 and 200 K. The exponent of the power law fits is 3.76, 2.5 and 1.87 for temperatures T_L = 200, 300 and 400 K, respectively, which is in agreement with the exponent T_H/T_L in Eq.(25). The power-law behavior resulting from the pivot effect is shown in the inset for T = 200 K.

The average boost can be derived in terms of the number of KMC events n from a potential energy basin B. The low temperature time after n events is given by $t_L = \sum_{p=1}^{n} -ln(\zeta_p)/k_{total,L,p}$, where ζ_p is a uniform distribution random variate and $k_{total,L,p}$ is the sum of process rates from the basin B at T_L after the p^{th} visit. Using Eq.(25) the average boost is

$$\begin{aligned}\langle B_{p-TAD}(n)\rangle &= \frac{\langle t_L(n)\rangle}{\langle t_{H,stop}(n)\rangle} \\ &= \frac{(\nu^*_{p-TAD})^{1-\beta_H/\beta_L}}{\alpha_w^{\beta_H/\beta_L}} \frac{n \sum_{p=1}^{n} 1/k_{total,L,p}}{\lim_{a\to 0} \int_a^1 \ldots \int_a^1 \left(\sum_{p=1}^{n} -ln(\zeta_p)/k_{total,L,p}\right)^{\beta_H/\beta_L} d\zeta_1 \ldots d\zeta_n}.\end{aligned} \tag{27}$$

Note that t_L and $t_{H,stop}$ are independent variables, so the averages are computed separately. The boost is lower when the sum of rates is large. This behavior, which is in common with the original TAD method, is observed when number of processes for the basin is large or when fast processes are present. This becomes more evident when $k_{total,L,p}$ is constant for all values of p, in which case the boost is proportional to $1/(k_{total,L,p})^{1-\beta_H/\beta_L}$.

VI. STUDY OF SUBMONOLAYER AG ON CU(110)

The p-TAD method can be used to study any arbitrarily complex material system that obeys the transition state theory. In this section, submonolayer Ag/Cu(110) is studied to highlight additional strengths of the p-TAD method in comparison to the conventional KMC approach. The alloy Ag in Cu is bulk immiscible and forms a eutectic mixture [27]. This is evident from the large mismatch in their lattice constants (12% mismatch), and in their surface energies and positive heat of mixing. The main applications of the Ag-Cu alloys are found in the electronics industry. In addition, the Ag-Cu system forms an ideal system for studying diffusion on surfaces and bulk. As a result, a number of experimental and theoretical studies of this material system have been undertaken [27–31]. Despite this, atomic processes predominant in Ag on Cu(110) surface have not been clearly understood [28, 32]. In Ref. [30], an alloy–de-alloy transition was experimentally observed as Ag was deposited on Cu(110) at submonolayer coverages. At low Ag coverages ($c_{Ag} < 0.4$ ML) the Ag adatoms substitutionally alloy into the Cu surface layer, forming a Cu-Ag alloy surface layer. Similar alloying behavior is also observed on other surfaces, such as Pb on Cu surfaces [33, 34]. Beyond $c_{Ag} = 0.65$ ML, surface alloying is not observed. Instead zig-zag chain nanostructures of Ag are formed pointing along the [100] direction. In this section, we perform p-TAD calculations at different submonolayer Ag thickness and substrate temperatures to elucidate the atomic processes involved that lead to the surface alloying and de-alloying and analyze the computational efficiency of the p-TAD method.

The minimum energy structures of Ag/Cu(110) thin films were identified at different Ag submonolayer coverages in order to test the EAM potential of Ref.[26]. The phase space was sampled starting from a randomly arranged Ag film with coverage c_{Ag}. The typical size of the Cu(110) surface used for the minimization procedure and the p-TAD simulation is shown in Fig. 7. Slab boundary conditions were employed. The energy minimization was performed by i) either displacing a randomly selected Ag atom along the surface or ii) randomly exchanging positions of a Ag atom and a Cu atom. After the move the energy of the entire system was minimized according using a steepest descent method [35]. The move was accepted according to a Metropolis criterion [36]. Other types of moves, such as exchange of 2 Cu atoms, were ignored since energy minimization of the Ag/Cu(110) structure was the only objective. The lowest energy configuration selected from 10000 steps are shown

in Fig. 7 for coverages ranging from 0.08-0.78 ML. At low coverages, e.g., 0.08 ML Ag, Ag adatoms replace surface Cu atoms forming a surface alloy. The energy change associated with surface alloying is -0.024 eV/Ag atom. The small change in energy suggests that entropic contributions can play an important role in Ag/Cu(110). At higher coverages ($0.19 - 0.63$ ML), it is observed that a subsurface Ag alloy coexists with Ag adatoms. The Ag adatoms minimize their energy by forming continuous chains along the $[1\bar{1}0]$ direction. Zig-zag chains are not observed due to the small size of the periodic box chosen. Due to the increasing compressive surface strain with increasing Ag coverage, Ag atoms are found on the Cu surface at $c_{Ag} = 0.78$. The conclusions made from the minimization procedure are in qualitative agreement with experimentally observed surface alloying–dealloying behavior [30].

The p-TAD method was employed to study the system evolution at $T_L = 150$ K and 300 K. The parameters employed were $\nu_{min} = 5 \times 10^{11}\ s^{-1}$, $\delta = 0.05$, $T_H = 750$ K and $4fs$ as the MD time step. A total of 10^{-4}-$10^{1}\ s$ was accessed at $T_L = 150$ K with 24 hours of CPU time for different Ag coverages studied in Fig. 6. On the other hand, $10^{-8} - 10^{-3}\ s$ was accessed at $T_L = 300$ K using roughly the same computational time. As evident from Section IV, longer times are accessed with similar CPU requirements for small values of temperature T_L. Low-barrier processes with large process rates are observed at high Ag coverages. This also increases the CPU requirements (see Eq. (27)). The alloying–dealloying phase separation behavior observed in the energy minimization procedure is also observed in the p-TAD calculations. Examples of some of the processes observed in the p-TAD calculations are shown in Figs.8-11. In each panel, the initial, saddle and final state are shown from left to right. For convenience, only a small number of atoms around the atoms participating in the process are shown. The arrows indicate direction in which participating atoms move. As discussed next, the p-TAD method overcomes several challenges associated with the KMC method that were outlined in the introduction.

The hopping and exchange mechanisms [33, 37, 38] are the most common processes observed in the p-TAD calculations. In a hop process (examples shown in Fig.8), a Ag or Cu atom (or multiple Ag and/or Cu atoms) located at a groove (grooves) hop along the $[1\bar{1}0]$ and $[\bar{1}10]$ directions. Single-atom and possibly even two-atom processes, such as the hop processes shown in Fig.8a and b are included in conventional KMC catalogs. In general, the rate and activation barrier for a process gets modified when the local arrangement of atoms, i.e., the local environment, around the atoms participant in the process is different. Conse-

quently, the minimum energy structure in terms of the position of all atoms in the system was used to obtain the current state of the system in the p-TAD implementation used here. A challenge that arises in multicomponent material simulations is that the number of processes and different local atomic arrangements that are possible increases in a combinatorial fashion with the system size and species type. As a result, estimating process rates *a priori* for different local environments becomes cumbersome with the conventional KMC catalog even if only simple types of processes are considered. This problem is solved in the p-TAD since the relevant *on-the-fly* KMC catalog is generated automatically. The computational cost associated with KMC process selection is reduced, since the list of processes is shorter and irrelevant processes are absent. Thus the p-TAD method provides a more systematic way for generating accurate process catalogs.

Few of the process activation barriers in Fig. 8-11 are large, implying that these processes are selected rarely at short time scales. Typically, large-barrier processes are rarely observed with direct MD based process detection techniques. On the other hand, the p-TAD method can easily detect both low and high barrier processes by studying dynamics in an efficient yet accurate manner. High activation barrier processes are selected more frequently in long KMC simulations and at high system temperatures. Further, in some cases even large-barrier processes can become important and may trigger an interesting behavior whenever they are selected (e.g., in crack propagation).

In the exchange mechanism (Fig.9), an adatom displaces a surface atom to take its place. The displaced surface atom becomes an adatom. These processes can also be incorporated in KMC process catalogs. However, many-atom processes (see exchange process in Fig.9b and c) and long-ranged processes (see exchange process in Fig.9d), where the displaced atom is a few lattice constants away from its initial position, are difficult to guess in the conventional KMC method. In Fig.9d, a long-ranged process is shown where the surface Cu atoms squeeze out one surface Cu atom, creating a Cu adatom. Simultaneously, the surface vacancy is filled up by a Ag atom. Long-ranged processes have been observed experimentally in many material systems (examples of long-ranged processes on (110) surfaces can be found in Ref. [39, 40]). In Fig.9f, an exchange move in shown where one of the Ag atoms ends up 2 layers above the Cu surface. This behavior adds more complexity to the KMC catalog. The solid-on-solid approximation is commonly used with the KMC method for studying multilayer thin films [41, 42], which typically assumes that only single-atom processes are

present.

In a cross-channel process (Fig. 10a), the participating atoms are displaced from one $[1\bar{1}0]$ channel to a neighboring channel. Many processes observed in the p-TAD calculations that have mixed features of different process mechanisms. These processes are many-atom processes and have a well-defined transition state. The process shown in Fig.8c is a four-atom process that combines hop and exchange mechanisms. Fig.9c is another such example. Fig.10b shows a 3-body cross-channel process resembling an exchange process that involves 2 Ag atoms and a Cu atom. Clearly, the p-TAD method overcomes challenges arising from finding relevant many-atom and/or long-ranged and/or mixed mechanism processes.

It is intuitively expected that all atoms in the submonolayer Ag/Cu(110) will reside in lattice positions, i.e., an adatom sits on top of 4 surface atoms. While this it true at low Ag coverages (c_{Ag} <), it is observed that the Ag atoms can reside in off-lattice positions at higher local Ag coverages (e.g., close to 1 monolayer) due to build-up of lattice-mismatch induced strain in the surface layers. Examples of such processes observed at $c_{Ag} \geq 0.53$ are shown in Fig.11 where the participating atoms which belong to the 2^{nd} above the Cu surface can sit on top of 3 surface atoms. At other regions with low local Ag coverage (e.g., < 0.7 monolayer), the Ag atoms reside in lattice sites. In such situations, on-lattice KMC schemes break down. This weakness of on-lattice KMC and the presence of surprising complex events was demonstrated previously in Ref. [7].

VII. CONCLUSIONS

In this paper, a variation of the TAD method, called the p-TAD method, is introduced for efficiently studying long-time dynamics with the accuracy of a MD simulation while assuming that transition state theory is valid. Applications of the method include solid-state materials modeling. The p-TAD method records processes detected in a high temperature basin-constrained MD (BCMD) simulation to efficiently generate an *on-the-fly* KMC process catalog. A p-TAD criterion is derived that specifies how long the BCMD calculation must be performed to guarantee that all processes from the basin that are *relevant* at the current time scales of the simulation have been found with a confidence $1 - \delta$. Here, δ gives the statistical error associated with a relevant process being missing from the KMC catalog. The dynamics is studied by sampling processes with a probability proportional to their rates

at the actual system temperature in the typical KMC way. An *on-the-fly* KMC process catalog is generated as new processes are detected in previously/newly visited basin by following the high temperature system dynamics. While in the previous TAD methods the dynamics was directly obtained by projecting high temperature escape times from the BCMD calculation by assuming harmonic transition state theory (HTST), in the p-TAD method the BCMD calculation is only employed to detect the relevant processes. Consequently, the p-TAD method can overcome the errors resulting from the HTST assumption in the previous TAD methods. Accurate dynamics is ensured by i) computing accurate rates at the system temperature and ii) introducing the anharmonicity allowance. Different ways of computing low temperature rate for newly detected processes can be employed depending on the accuracy needs and computational limitations. Furthermore, DFT or more accurate potentials can provide a more accurate process rates. As a result, even quantum effects such as tunneling can be incorporated.

The KMC process catalog generated using p-TAD method can be reused for future p-TAD calculations. In such cases, the cost of the p-TAD method equals that of a KMC method provided that the basins that are visited were already observed in the p-TAD calculations that generated the process catalog. Effective confidence measures derived in Section IV can provide an estimate of the resulting accuracy of the KMC catalog when the catalog is used for conditions different from the ones it was generated for. The p-TAD method also enables use of parallel computing to accelerate the generation of process catalog. KMC catalogs from different p-TAD calculations can be updated and merged with knowledge of the resulting catalog accuracy, a feature that is extremely useful for developing generic KMC databases.

Studies performed in this paper on Ag/Ag(100) and Ag/Cu(110) demonstrate that the accuracy and computational requirements of the p-TAD method can be easily controlled by tuning the confidence levels and the temperature for the BCMD calculation. Tremendous computational boost up to 10^{10} were obtained. It is shown that that most atomistic processes and off-lattice behavior encountered in the p-TAD calculations for Ag/Cu(110) cannot be intuitively guessed. The p-TAD method overcomes several challenges encountered in the conventional KMC method. It was shown that the p-TAD method is an ideal tool for accurately and efficiently generating relevant KMC process catalogs for complex materials, such as multicomponent and strained systems.

VIII. ACKNOWLEDGEMENTS

This work was supported by the United States Department of Energy, Office of Basic Energy Sciences and Division of Materials Sciences and Engineering. AC acknowledges funding from Director's postoctoral fellowship at the Los Alamos National Laboratory (LANL). LANL is operated by Los Alamos National Security, LLC, for the National Nuclear Security Administration of the U.S. Department of Energy under contract DE-AC52-O6NA25396.

---

[1] D. Gillespie, J. Comp. Phys. **22**, 403 (1976).

[2] A. Bortz, M. Kalos, and J. Lebowitz, J. Comp. Phys. **17**, 10 (1975).

[3] A. Voter, *Radiation Effects in Solids*, chapter Introduction to the kinetic Monte Carlo method, pages 1–23, Springer Netherlands, 2007.

[4] A. Chatterjee and D. Vlachos, J. Comput. Aided Mater. Des. **14** (2007).

[5] H. Kramers, Physica **7**, 284 (1940).

[6] P. Hänggi, P. Talkner, and M. Borkovec, Rev. Mod. Phys. **62**, 251 (1990).

[7] G. Henkelman and H. Jónsson, J. Chem. Phys. **115**, 9657 (2001).

[8] A. Voter, Phys. Rev. B **34**, 6819 (1986).

[9] G. Henkelman and H. Jónsson, J. Chem. Phys. **111**, 7010 (1999).

[10] O. Trushin, A. Karim, A. Kara, and T. Rahman, Phys. Rev. B **72**, 115401 (2005).

[11] A. Voter, F. Montalenti, and T. Germann, Ann. Rev. Mat. Res. **32**, 321 (2002).

[12] M. Sorensen and A. Voter, J. Chem. Phys. **112**, 9599 (2000).

[13] M. Allen and D. Tildesley, *Computer simulation of liquids*, Oxford Science Publications, Oxford, 1989.

[14] F. Montalenti and A. Voter, J. Chem. Phys. **116**, 4819 (2002).

[15] Y. Shim, J. Amar, B. Uberuaga, and A. Voter, Phys. Rev. B **76**, 205439 (2007).

[16] J. Sprague, F. Montalenti, B. Uberuaga, J. D. Kress, and A. F. Voter, Phys. Rev. B **66**, 205415 (2002).

[17] F. Montalenti, M. R. Sørensen, and A. F. Voter, Phys. Rev. Lett. **87**, 126101 (2001).

[18] K. Sickafus, W. Weber, and B. Uberuaga, Nucl. Instr. and Meth. B **250**, vii (2006).

[19] B. Uberuaga et al., Phys. Rev. B **71**, 104102 (2005).

[20] N. Van Kampen, *Stochastic processes in physics and chemistry*, North-Holland personal library, 1992.

[21] G. Vineyard, J. Phys. Chem. Solids **3**, 121 (1957).

[22] H. Jónsson and G. Mills, Nudged elastic band methods for finding minimum energy paths of transitions, in *Classical and Quantum Dynamics in Condensed Phase Simulations*, edited by B. Berne, G. Ciccotti, and D. Coker, pages 385–404, Singapore, World Scientific, 1998.

[23] P. Hohenberg and W. Kohn, Phys. Rev. **136**, B864 (1964).

[24] W. Kohn and L. Sham, Phys. Rev. **140**, A1133 (1965).

[25] R. Car and M. Parrinello, Phys. Rev. Letters **55**, 2471 (1985).

[26] P. Williams, Y. Mishin, and J. Hamilton, Modell. Simul. Mater. Sci. Eng. **14** (2006).

[27] C. Vardeman and J. Gezelter, J. Phys. Chem. A **105**, 2568 (2001).

[28] U. Kurpick, M. G., and G. A., Appl. Surf. Sc. **89**, 383 (1995).

[29] H. Chen and J.-M. Zuo, Acta Mat. **55**, 1617 (2007).

[30] . Kizilkaya et al., Surface Science **596**, 242 (2005).

[31] I. Meunier, R. Tetot, G. Treglia, and B. Legrandc, Appl. Surf. Sci. **177**, 252 (2001).

[32] T. Taylor, M. Hoffbauer, C. Maggiore, and J. Beery, J. Vac. Sci. Tech. A **5**, 1625 (1987).

[33] G. Prevot, C. Cohen, J. Moulin, and D. Schmaus, Surface Science **421**, 364 (1999).

[34] C. Nagl, E. Platzgummer, O. Haller, S. M., and P. Varga, Surface Science **331-333**, 831 (1995).

[35] W. H. Press, B. P. Flannery, S. A. Teukolsky, and W. T. Vetterling, *Numerical Recipes*, Cambridge University Press, Cambridge, 1986.

[36] N. Metropolis, A. Rosenbluth, M. Rosenbluth, A. Teller, and E. Teller, J. Chem. Phys. **21**, 1087 (1953).

[37] P. Feibelman, Phys. Rev. Lett. **65**, 729 (1990).

[38] J. Wrigley and G. Ehrlich, Phys. Rev. Lett. **44**, 661 (1980).

[39] G. Antczak and G. Ehrlich, J. Colloid Interface Sci. **276**, 1 (2004).

[40] T. Linderoth, S. Horch, E. Lægsgaard, I. Stensgaard, and F. Besenbacher, Phys. Rev. Lett. **78**, 4978 (1997).

[41] H. Muller-Krumbhaar, *Current topics in material science*, chapter Kinetics of crystal growth, pages 1–46, North-Holland, 1978.

[42] G. Gilmer, Science **208**, 355 (1980).

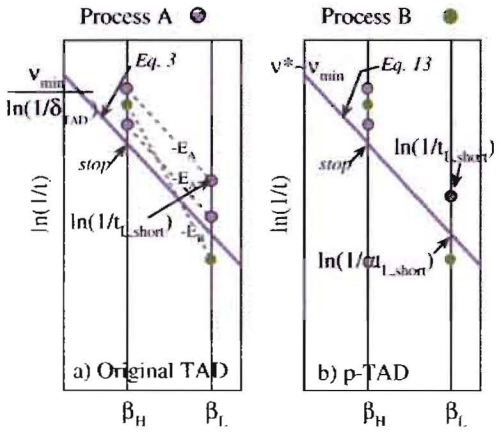

FIG. 1: Schematic of a basin-constrained molecular dynamics (BCMD) calculation performed during the first visit to a particular basin with the a) original TAD and b) p-TAD method. The two methods can i) detect processes in the basin at the current time scales of the simulation and then ii) study the dynamics by selecting the process with the shortest escape time $t_{L,short}$ at β_L for studying the system dynamics. Processes A and B are detected in the BCMD calculation. In original TAD method, each process escape time recorded in the high temperature BCMD calculation is projected (dashed lines) to obtain the low temperature escape time using Eq. (3). In p-TAD method, a low temperature escape time is sampled from Eq.(1) for a new process. The stopping criterion (bold line) specifies the duration of the BCMD calculation, such that the process with the shortest time in original TAD or a list of relevant processes in p-TAD is guaranteed to be found with a chosen confidence. See text for steps involved in future revisits to the same basin.

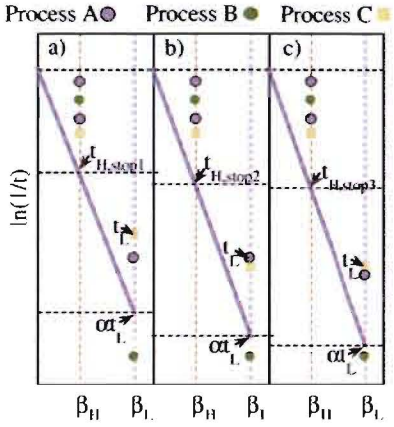

FIG. 2: A p-TAD calculation is shown for 3 visits to the same basin B. a) In the first visit process A, B and C are detected in the BCMD calculation. Corresponding escape times are sampled at low temperature probability from Eq. (1). Process C has shortest escape time $t_{L,C}$ and the BCMD stop time $t_{H,stop1}$ is computed from $t_{L,C}$. Process C is selected and the system jumps to a different basin. A new escape time $t_{L,C}$ is sampled for selected process C for the next visit to the basin B. b) When the trajectory returns to B, the stop time $t_{H,stop2}$ is computed from the shortest escape time given by $t_{L,A}$. Process A is selected after ensuring that no new process is detected during the BCMD calculation from time $t_{H,stop1}$ to $t_{H,stop2}$. A new escape time $t_{L,A}$ is sampled for the selected process A. The duration of the BCMD calculation decreases in a power-law fashion as more time is spent in the basin. Whenever a new process was detected in the BCMD calculation, the process is added to the KMC catalog and its escape time is sampled from Eq. (1). The stop time is recomputed from the shortest escape time. c) Same procedure is followed for future revisits to basin B.

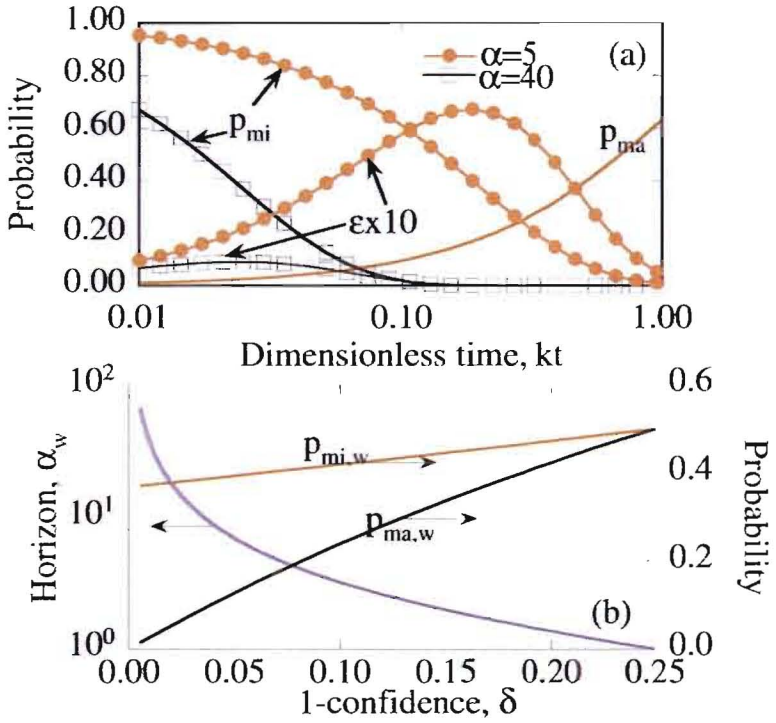

FIG. 3: a) The probability p_{ma} of observing a process with rate k before low temperature dimensionless time kt, probability p_{mi} of observing the same process after time αkt are shown. The probability $\epsilon = p_{mi}p_{ma}$ gives an error measure associated with not including a process in the KMC catalog. b) The horizon α_w, and probabilities $p_{ma,w}$ and $p_{mi,w}$ are plotted against the confidence measure $1 - \delta$.

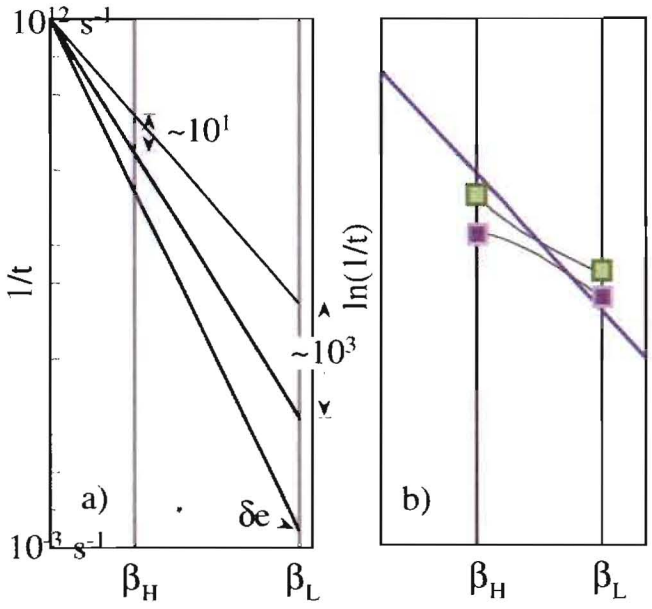

FIG. 4: a) Example of the sweeping effect in the p-TAD method. The p-TAD parameters used are $\beta_L = 300$ K, $\beta_H = 900$, $\nu_{min} = 10^{12}\ s^{-1}$ and $\delta = 0.01$. Three-orders of magnitude low temperature time is swept for every order of magnitude BCMD time studied. b) In certain cases as shown, a process relevant to the KMC catalog is not detected in the BCMD calculation due to anharmonicity effects.

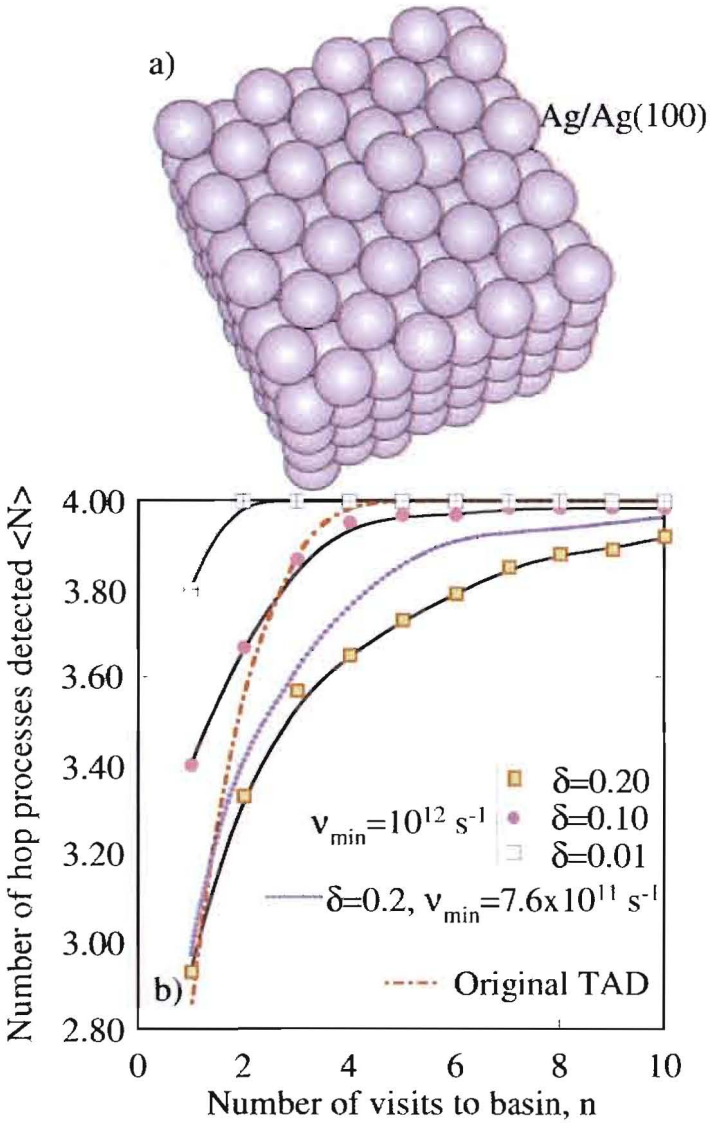

FIG. 5: a) Ag adatom on Ag(100) system studied with the p-TAD method. b) The addition of 4-symmetrically equivalent hop processes to the KMC catalog for different p-TAD parameters. Temperatures $T_H = 750$ K and $T_L = 400$ K are used. For calculations with $\delta = 0.2, 0.1, 0.01$, $\nu_m in$ is $10^{12}\ s^{-1}$. In the original TAD calculation, $\nu_m in = 10^{12}\ s^{-1}$. Results from a p-TAD calculation with $\delta = 0.2$ and $\nu_{min} = 7.6 \times 10^{11}\ s^{-1}$ are also shown.

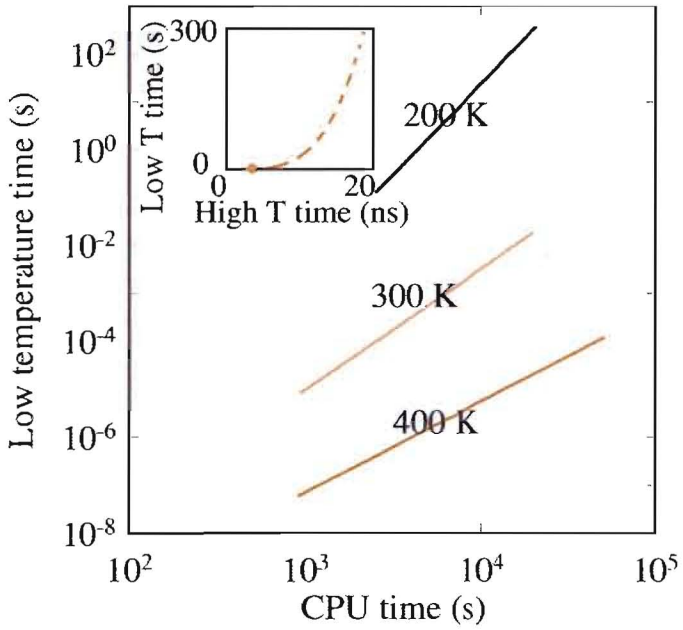

FIG. 6: Computational requirements for the p-TAD method. Lines correspond to power law fit. The power-law growth in low temperature time with respect to the BCMD time for $T_L = 200$ K is shown in the inset. An open circle is shown for every 100^{th} KMC move, while the first KMC move is denoted by a filled circle.

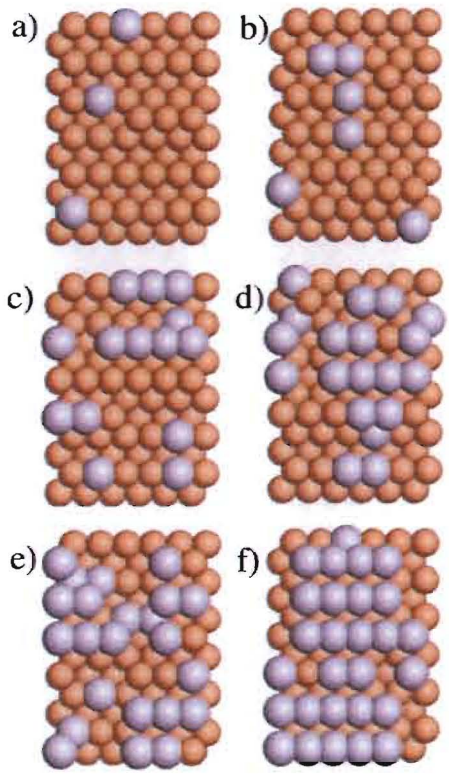

FIG. 7: Lowest energy structures obtained using the minimization procedure described in text at different Ag/Cu(110) coverages. Ag (Cu) is shown in blue (brown) color. The sampling method is described in the text. 10000 configurations were sampled for each Ag coverage. Structures shown in a-f correspond to Ag coverage $c_{Ag} = 0.08$, 0.19, 0.39, 0.53, 0.64 and 0.78.

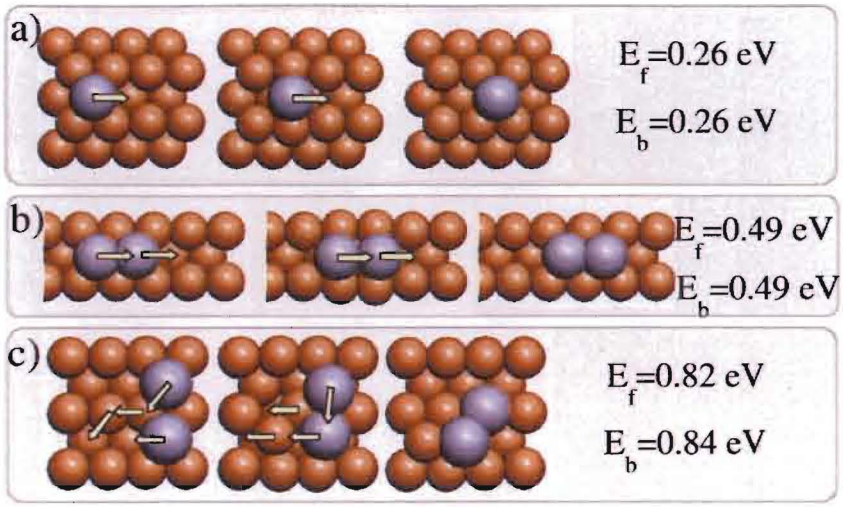

FIG. 8: Examples of different hopping processes observed in the p-TAD calculations of Ag/Cu(110). Blue (brown) circles correspond to Ag (Cu) atoms. See text for more details.

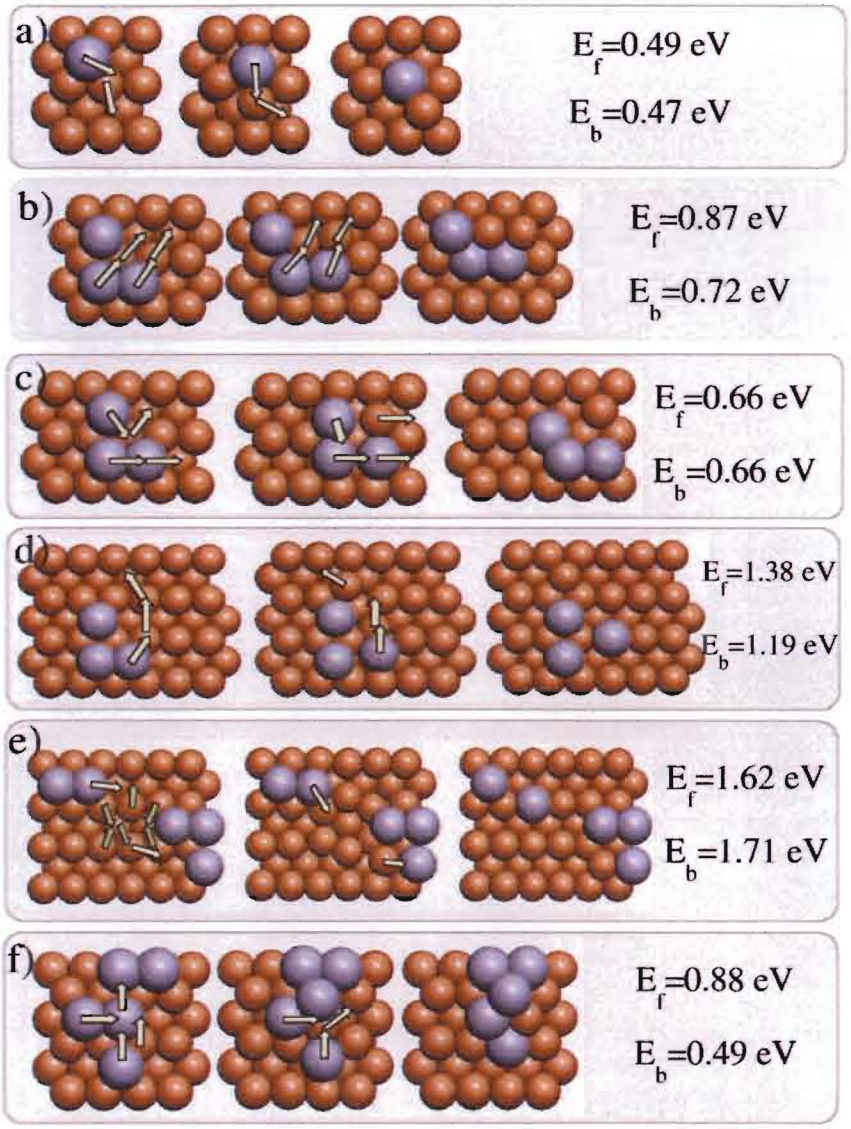

FIG. 9: Examples of different exchange processes observed in the p-TAD calculations of Ag/Cu(110). Blue (brown) circles correspond to Ag (Cu) atoms. See text for more details.